IEEE Access
Multidisciplinary : Rapid Review : Open Access Journal

Received 31 March 2023, accepted 7 April 2023, date of publication 12 April 2023, date of current version 24 April 2023.

Digital Object Identifier 10.1109/ACCESS.2023.3266522

RESEARCH ARTICLE

Fault Diagnosis Based Machine Learning and Fault Tolerant Control of Multicellular Converter Used in Photovoltaic Water Pumping System

B. ROUABAH[1], H. TOUBAKH[1], M. DJEMAI[2,3], (Senior Member, IEEE), L. BEN-BRAHIM[4], (Senior Member, IEEE), AND RAYMOND GHANDOUR[5], (Senior Member, IEEE)

[1]Department of Electronic and Telecom, FNTIC Faculty, University of Kasdi Merbah Ouargla, Ouargla 30000, Algeria
[2]INSA Hauts-de-France, LAMIH UMR CNRS 820, UPHF, Campus Mont Houy, 59300 Valenciennes, France
[3]QUARTZ Laboratory EA 7393, ENSEA Cergy, 95000 Cergy, France
[4]Electrical Engineering Department, Qatar University, Doha, Qatar
[5]College of Engineering and Technology, American University of Middle East, Egaila 54200, Kuwait

Corresponding author: B. Rouabah (rouabah.boubakeur@univ-ouargla.dz)

This work was supported in part by the QUARTZ Laboratory Cergy, France, and in part by the College of Engineering and Technology, American University of Middle East, Egaila, Kuwait.

ABSTRACT Currently, providing water in developing countries, especially in dry and hot rural areas, is a significant challenge. However, creating new electric grids is often expensive. Therefore, the use of low-cost photovoltaic (PV) panels in water pumping systems, without chemical energy storage, based on high-performance and more efficient power converters with increased time life and lower maintenance interventions is needed. In this study, a photovoltaic water pumping system with two power converters, the first is used to extract the maximum power using the maximum power point tracking (MPPT) algorithm, and the second is a three-cell multicellular power converter used to control the DC motor with a submerged pump. Meanwhile, the serial connection and redundant topology of multicellular converters render the system more vulnerable to failure. fault diagnosis-based machine learning approach and fault tolerant control (FTC) are proposed for multicellular power converters. Simulation results with MATLAB show the effectiveness and practicability of the proposed structure and control to isolate the faulty capacitor, increase the sustainability of the system, assure the supply of water under faulty conditions, minimize the mechanical vibrations in electric DC motors, and avoid PV system shutdown.

INDEX TERMS Photovoltaic water pumping system, multicellular converter, fault diagnosis based machine learning, fault tolerant control (FTC).

I. INTRODUCTION

A. MOTIVATION

The most important characteristic of isolated sites in deserts is the dry and hot climate, scarcity of water, unpredictable rainfall, and plentiful sunshine. As the water is indispensable, the lives of inhabitants of these desert regions are threatened. Pumping water from the deep soil layer is considered a reliable solution for providing water. However, this solution requires an external power source [1]. Owing to the high cost of electric grids in isolated desert, rural, and agricultural sites, photovoltaic energy has become the optimal solution as it is environmentally friendly, has fewer maintenance coasts, and is freely available [2]. Therefore, at isolated sites, photovoltaic (PV) panels are used in pumping systems for irrigation and potable water. Power electronic converters are used in solar energy conversion as an interface between PV panels and electric loads, and their efficiency depends on the type and state of health of the power converter. However, most power converters require a large number of power switches and power capacitors, which makes the system more susceptible to the occurrence of faults. Therefore, fault diagnosis and fault-tolerant control are necessary to ensure high performance of the power converter.

The associate editor coordinating the review of this manuscript and approving it for publication was Guillermo Valencia-Palomo.

B. RELATED WORKS

In [1], a sizing study to increase the performance of a solar photovoltaic water pumping system in any season or under any climatic conditions was conducted, and in [3], a technical, economic, and social approach for the optimal design of photovoltaic water pumping systems for rural communities was proposed. Different topologies of power converters are used in PV systems to enhance the reliability and efficiency of solar energy systems based on PV panels. a DC/DC classic converter is used in water pumping system based on photovoltaic panels is used in [4], a classical two-level topology is used in [5] and [6] for PV water pumping system in rural areas. However, a considerable voltage stress on switching devices in the classical two-level topology and high dv/dt ratio increases the power loss and can cause damage to switching devices [7], [8]. Therefore, a multilevel converter topology is proposed in a PV water pumping system [9] that can operate with low-voltage stress across devices and a wide voltage range. Among multilevel topologies, a multicellular converter which has more advantages such as can operate under high DC voltage, lower rating power switches [10], [11], [12], [13], increased switching frequency, reduced voltage stress, and adjustable output voltage [14], [15]. In [16], a multicellular converter with a new Maximum Power Point Tracking (MPPT) algorithm was used in photovoltaic applications. However, a failure in flying capacitors should eliminate all the advantages of multicellular topology, reduce the power quality, affect the power transmission from the PV panel to the electric motor, and increase the mechanical and thermal stresses in electric motors. Therefore, the use of fault diagnosis and fault tolerant control (FTC) is necessary to isolate faults and maintain the stability of PV systems and electric motors. In [17], [18], and [19], fault diagnosis-based machine learning was used to detect the failure of flying capacitors and power switches in multicellular converters.

C. CONTRIBUTION

In this study, a photovoltaic water-pumping system based on two power converters is proposed. The first is used for the MPPT algorithm, and the second is a three-cell multicellular converter used to control the DC submerged pump. In order to ensure high performance of the proposed system, a fault diagnosis-based machine learning approach is used. Fault-tolerant control applied to multicellular power converters allows the isolation of failures and maintain the operation of the proposed system with minimum mechanical vibration, reduced heating stress, and increased lifetime of the DC motor windings. The effectiveness and practicability of the proposed structure are verified via simulation.

This paper is organized as follows: In section II, the modeling of photovoltaic panels with the MPPT algorithm is described. Section III describes multicellular converter modeling and control using the sliding mode approach in different operating modes (healthy and faulty modes). Fault diagnosis using a machine-learning approach is considered in Section 4. Fault-tolerant control is detailed in Section 5. Finally, Section 6 concludes the paper.

Figure 1 illustrates the proposed structure.

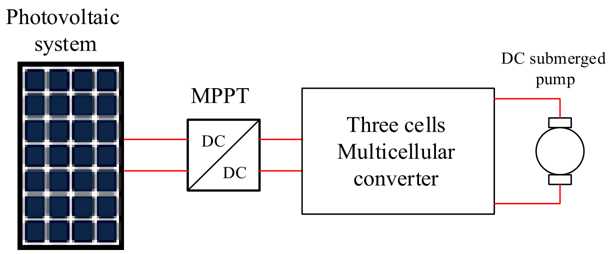

FIGURE 1. Proposed topology of water pumping system.

D. PHOTOVOLTAIC SYSTEM

The equivalent electric circuit and modeling of the PV system are illustrated and detailed in references [16] using the following equation:

$$I_{pv} = I_{sc}[1 - k_1(\exp(\frac{V_{pv}}{k_2 V_{oc}}))] \tag{1}$$

With:

$$\begin{cases} k_1 = (1 - \frac{I_{MPP}}{I_{sc}})\exp(-\frac{V_{MPP}}{k_2 V_{oc}}) \\ k_2 = \dfrac{(\frac{V_{MPP}}{V_{oc}} - 1)}{\ln(1 - \frac{I_{MPP}}{I_{sc}})} \end{cases} \tag{2}$$

The MPPT control based on the P&Os algorithm applied to the DC/DC converter is described in the flowchart in Figure 3.

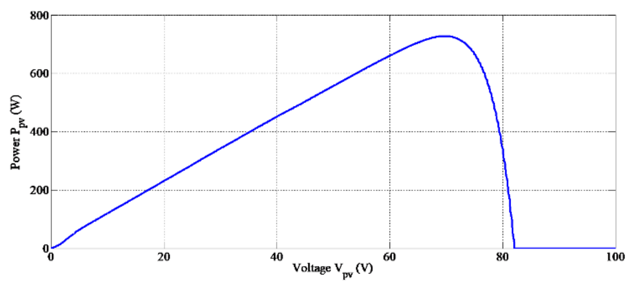

FIGURE 2. Power–voltage characteristic curve of a PV panels.

II. MODELING AND CONTROL OF MULTICELLULAR CONVERTER AND DC MOTOR

Figure.4 shows a three-cell DC/DC multicellular converter and DC motor.

The electromagnetic force E_m of DC motor is:

$$E_m = K_\varphi \Omega \tag{3}$$

The currents in flying capacitor $C1 = C2 = C$ can be expressed as:

$$\begin{aligned} i_{C1} &= C\frac{d}{dt}V_{C1} \\ i_{C2} &= C\frac{d}{dt}V_{C2} \end{aligned} \tag{4}$$

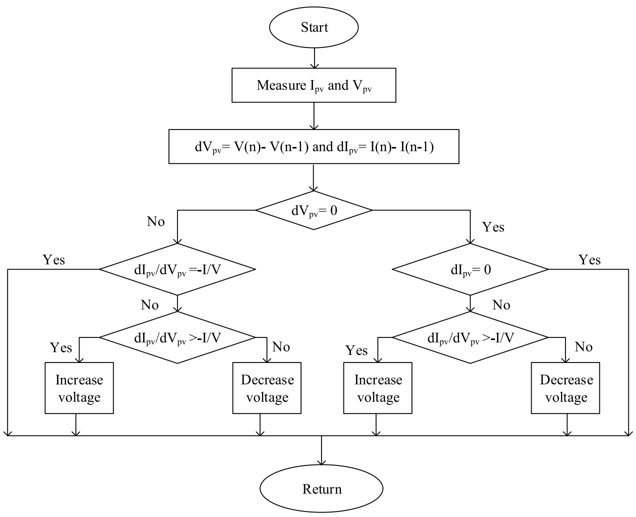

FIGURE 3. P & O algorithm.

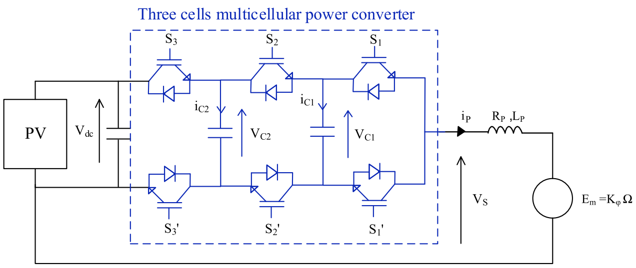

FIGURE 4. Multicellular converter topology.

The voltages of flying capacitors are given by:

$$\frac{d}{dt}V_{C1} = \frac{1}{C}[S_2 - S_1]$$
$$\frac{d}{dt}V_{C2} = \frac{1}{C}[S_3 - S_2] \tag{5}$$

According to the Figure.1 we can write the output voltage of multicellular converter V_S

$$V_S = S_1 V_{C1} + S_2[V_{C2} - V_{C1}] + S_3[V_{dc} - V_{C2}] \tag{6}$$

And the filter current i_f can be expressed as:

$$\frac{di_P}{dt} = \frac{1}{L_P}\left(S_1 V_{C1} + S_2\left[V_{C2} - V_{C1}\right] + S_3\left[V_{dc} - V_{C2}\right]\right) - \frac{R_P}{L_P}i_P - \frac{K_\varphi}{L_P}\boldsymbol{\Omega} \tag{7}$$

The nonlinear form of proposed structure is:

$$\begin{bmatrix} \dot{V}_{C1} \\ \dot{V}_{C2} \\ \dot{i}_P \end{bmatrix} = \begin{bmatrix} 0 & 0 & 0 \\ 0 & 0 & 0 \\ 0 & 0 & \frac{-R_P}{L_P} \end{bmatrix} \begin{bmatrix} V_{C1} \\ V_{C2} \\ i_P \end{bmatrix} + \begin{bmatrix} \frac{-i_P}{C} & \frac{i_P}{C} & 0 \\ 0 & \frac{-i_P}{C} & \frac{i_P}{C} \\ \frac{V_{C1}}{L_P} & \frac{V_{C2} - V_{C1}}{L_P} & \frac{V_{dc} - V_{C2}}{L_P} \end{bmatrix} \begin{bmatrix} S_1 \\ S_2 \\ S_3 \end{bmatrix} + \begin{bmatrix} 0 \\ 0 \\ -\frac{K_\varphi}{L_P}\boldsymbol{\Omega} \end{bmatrix} \tag{8}$$

The mechanical equation of DC motor is:

$$J\frac{d\Omega}{dt} = K_\varphi i_P - f\Omega - T_r \tag{9}$$

A. SLIDING MODE CONTROL OF MULTICELLULAR CONVERTER WITH DC MOTOR

The nonlinear model of multicellular converter in equation 8 can be written as:

$$\dot{x} = \mathrm{f}(x) + \mathrm{g}(x)\,\mathrm{u} + \mathrm{H} \tag{10}$$

With

$$\mathrm{x} = \begin{bmatrix} \mathrm{V_{C1}} \\ \mathrm{V_{C2}} \\ \mathrm{i_P} \end{bmatrix}, \quad \mathrm{f}(\mathrm{x}) = \begin{bmatrix} 0 & 0 & 0 \\ 0 & 0 & 0 \\ 0 & 0 & \frac{-\mathrm{R_P}}{\mathrm{L_P}} \end{bmatrix},$$

$$\mathrm{g}(\mathrm{x}) = \begin{bmatrix} \frac{-\mathrm{i_P}}{\mathrm{C}} & \frac{\mathrm{i_P}}{\mathrm{C}} & 0 \\ 0 & \frac{-\mathrm{i_P}}{\mathrm{C}} & \frac{\mathrm{i_P}}{\mathrm{C}} \\ \frac{\mathrm{V_{C1}}}{\mathrm{L_P}} & \frac{\mathrm{V_{C2}} - \mathrm{V_{C1}}}{\mathrm{L_P}} & \frac{\mathrm{V_{dc}} - \mathrm{V_{C2}}}{\mathrm{L_P}} \end{bmatrix}, \quad \mathrm{u} = \begin{bmatrix} \mathrm{S_1} \\ \mathrm{S_2} \\ \mathrm{S_3} \end{bmatrix}$$

and

$$\mathrm{H} = \begin{bmatrix} 0 \\ 0 \\ -\frac{\mathrm{K_\varphi}}{\mathrm{L_P}}\Omega \end{bmatrix}, \quad \mathrm{x_{ref}} = \begin{bmatrix} \frac{\mathrm{V_{dc}}}{3} \\ \frac{2\mathrm{V_{dc}}}{3} \\ \mathrm{i_{Pref}} \end{bmatrix}$$

The error vector is expressed as:

$$\mathrm{e} = \mathrm{x_{ref}} - \mathrm{x} = \begin{pmatrix} \frac{\mathrm{V_{dc}}}{3} - \mathrm{V_{C1}} \\ \frac{2\mathrm{V_{dc}}}{3} - \mathrm{V_{C2}} \\ \mathrm{i_{Pref}} - \mathrm{i_p} \end{pmatrix} \tag{11}$$

This error e is considered to be the sliding surface of the sliding mode control, with V is the Lyapunov function.

$$\mathrm{V} = \frac{1}{2}\mathrm{e^T e} \tag{12}$$
$$\dot{\mathrm{V}} = \mathrm{e^T}\dot{\mathrm{e}} \tag{13}$$
$$\dot{\mathrm{V}} = \mathrm{e^T}(\dot{\mathrm{x}} - \dot{\mathrm{x}}_{\mathrm{ref}})$$
$$\dot{\mathrm{V}} = \mathrm{e^T}(\mathrm{f}(\mathrm{x}) + \mathrm{g}(\mathrm{x})\,\mathrm{u} + \mathrm{H} - \dot{\mathrm{x}}_{\mathrm{ref}}) \tag{14}$$

Control low of sliding mode control is given by:

$$\mathrm{u} = \mathrm{u_{eq}} + \mathrm{u_n} \tag{15}$$

$\mathrm{u_n}$ is the sliding surface sign function and $\mathrm{u_{eq}}$ is the control input, which forces the state variables to the origin (zero error) on the sliding surface.

The equivalent $\mathrm{u_{eq}}$ control led to $\mathrm{e} = 0$ and $\dot{e} = 0$.

So,

$$\mathrm{u_{eq}} = -(\mathrm{g}(\mathrm{x}))^{-1}(\mathrm{f}(\mathrm{x}) + \mathrm{H} - \dot{\mathrm{x}}_{\mathrm{ref}}) \tag{16}$$

$$u = -(g(x))^{-1}(f(x) + H - \dot{x}_{ref}) + u_n \tag{17}$$

Substitution of equation 16 in equation 13

$$\dot{V} = e^T g(x)\, u_n \tag{18}$$

$$\dot{V} = e^T \left[\left(\frac{i_P}{C} + \frac{V_{C1}}{L_P} \right) S_1 + \left(\frac{i_P}{C} - \frac{i_P}{C} + \frac{V_{C2} - V_{C1}}{L_P} \right) S_2 + \left(\frac{i_P}{C} + \frac{(V_{dc} - V_{C2})}{L_P} \right) S_3 \right] \tag{19}$$

Toassure the Lyapunov stability the derivative of V must be negative.

$$S_1 = -\mathrm{sign}\left[e^T \left(\frac{i_P}{C} + \frac{V_{C1}}{L_P} \right) \right]$$
$$S_2 = -\mathrm{sign}\left[e^T \left(\frac{i_P}{C} - \frac{i_P}{C} + \frac{V_{C2} - V_{C1}}{L_P} \right) \right]$$
$$S_3 = -\mathrm{sign}\left[e^T \left(\frac{i_P}{C} + \frac{(V_{dc} - V_{C2})}{L_P} \right) \right] \tag{20}$$

the sliding mode control of multicellular converter is represnted in the figure 2

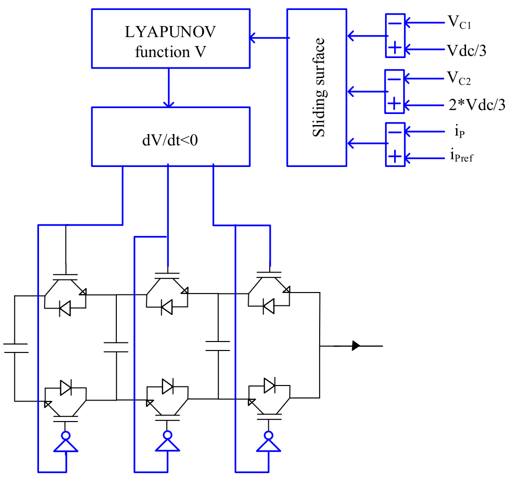

FIGURE 5. Sliding mode control of shunt active power filter.

Parameters simulation are given in table.1

TABLE 1. Simulation parameter.

Parameter	Value
V_{dc}	*220V*
R_P and L_P	*0.5Ω and 1.2mH*
C	*40μF*
K_φ	*0.9*
Ω_{ref}	*100 rad/S*

B. HEALTHY MODE

The simulation results of the healthy mode (Figure 6 to Figure 9) show that the flying capacitor voltages regulate at their references, the angular speed is equal to 100 rad/s, and the electromagnetic torque is equal to the resistant torque.

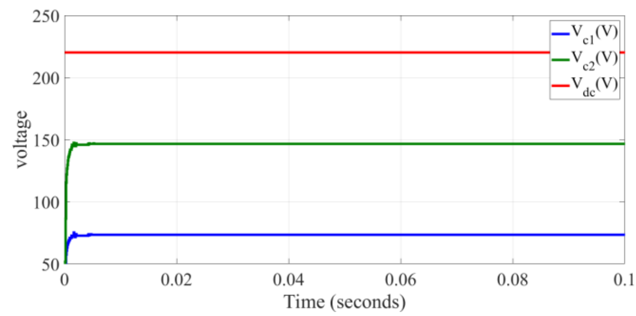

FIGURE 6. Flying capacitor voltages and DC side voltage in healthy mode.

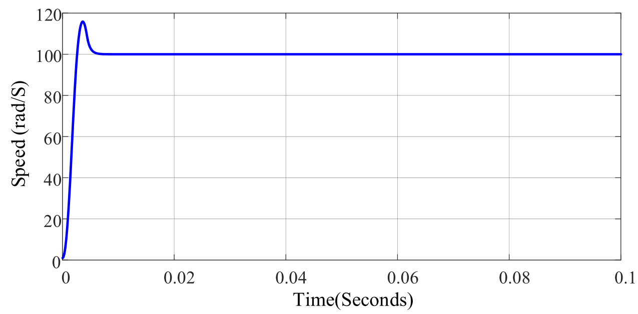

FIGURE 7. Angular speed of DC motor in healthy mode.

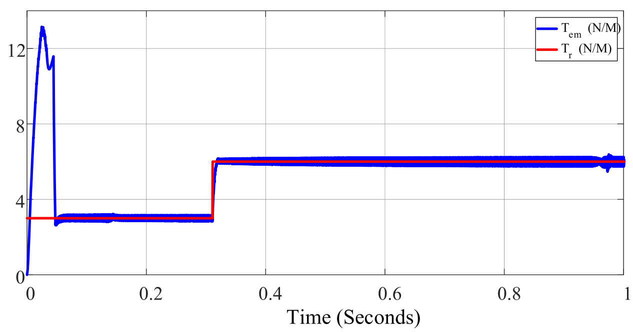

FIGURE 8. Electromagnetic torque and resistant torque in healthy mode.

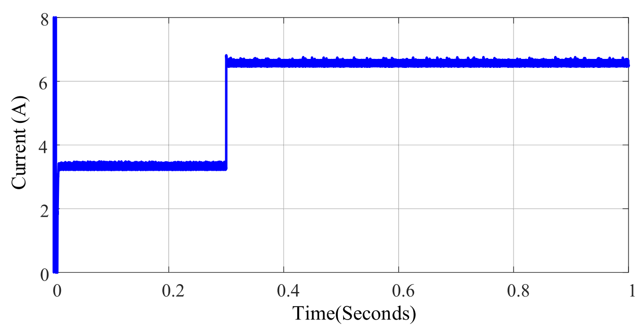

FIGURE 9. DC motor current in healthy mode.

C. ONE CAPACITOR FAILURE

In this part, the flying capacitor C_2 is defected at instant 0.5 S, as presented in Figure 10, the flying capacitor voltages are not regulated to their references (Figure.11), the angular speed diverges from 100 rad/S ($\Delta\Omega = 2.5rad/S$), and the electromagnetic torque and DC motor currant show large variations (ΔT_{em}= 10 NM, Δi_p= 10A).

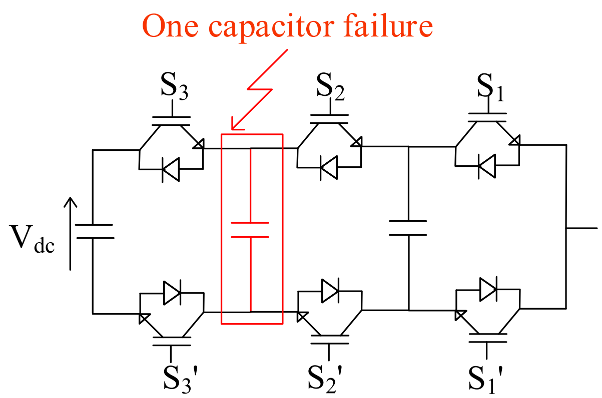

FIGURE 10. One capacitor failure.

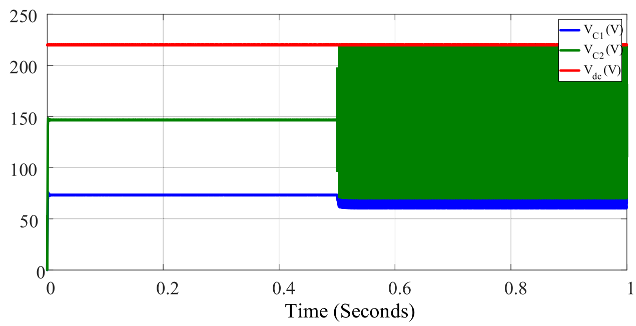

FIGURE 11. Flying capacitor voltages and DC side voltage in one capacitor failure mode.

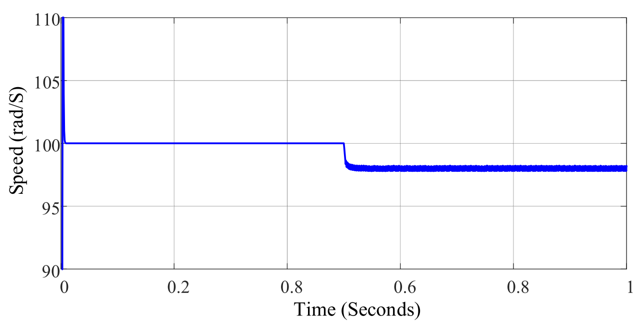

FIGURE 12. Angular speed of DC motor in one capacitor failure mode.

These results demonstrate that the defects of one flying capacitor in a multicellular converter cause mechanical vibrations and current harmonics in stator windings.

D. CAPACITOR FAULTS

The multicellular converter has two defective flying capacitors, as shown in figure.15

Figure 16 shows the V_{dc} and flying capacitor voltages, which deviate from their references, and the angular speed is

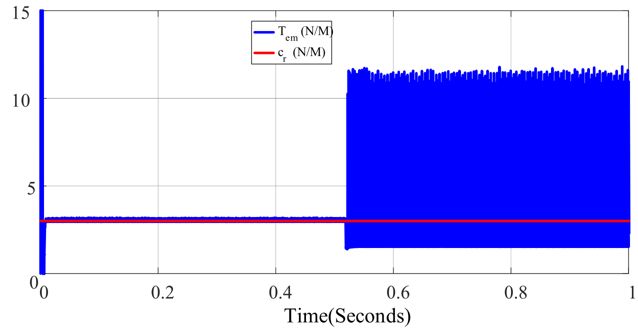

FIGURE 13. Electromagnetic torque and resistant torque in one capacitor failure mode.

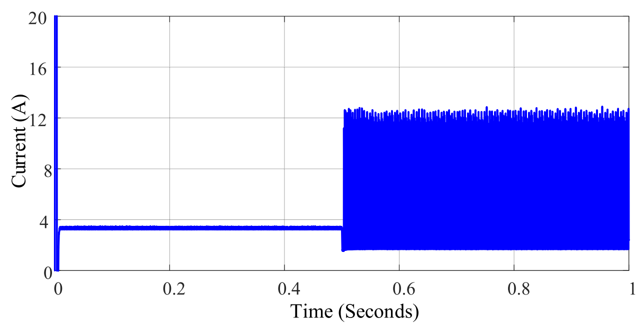

FIGURE 14. DC motor current in one capacitor failure mode.

$\Delta\Omega = 80rad/S$ (Figure 17). The electromagnetic torque and stator current exhibit a large variation from their references with (ΔT_{em}= 7 NM, Δi_p= 7A).

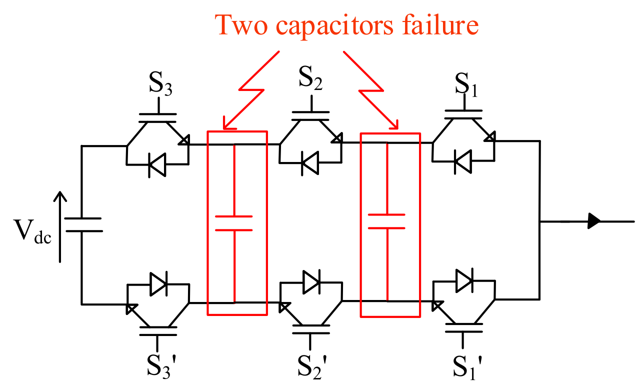

FIGURE 15. Two capacitors failure.

Current harmonics in electric machines create a flux harmonic in the magnetic core, which induces the circulation of harmonic currents in rotor and stator windings. The interaction between harmonic flux and harmonic current generates harmonic torque and vibrations [7]. In an electric rotating machine, the mechanical vibrations have the same frequency as the current harmonics [20], [21]. Because the current harmonics are multiples of the fundamental frequency (high frequency), mechanical vibrations also have a high frequency. Moreover, according to [22], fatigue problems are proportional to the frequency of the mechanical vibrations.

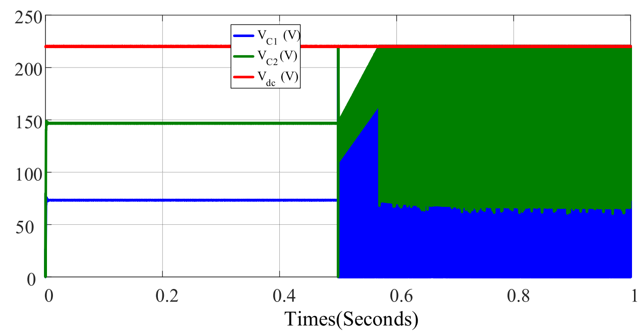

FIGURE 16. Flying capacitor voltages and DC side voltage in two capacitors failure mode.

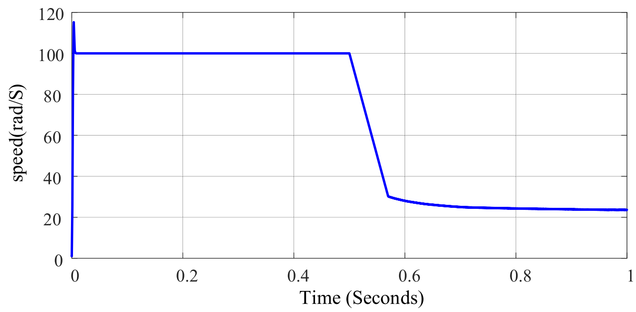

FIGURE 17. Angular speed of DC motor in two capacitors failure mode.

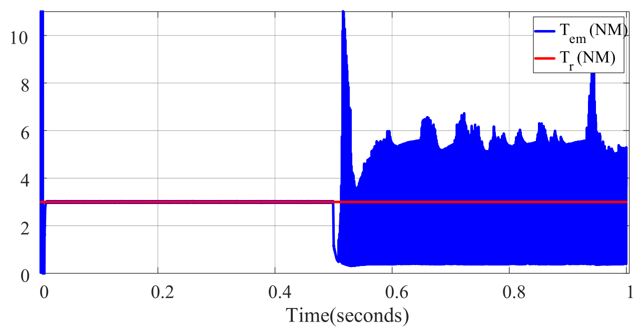

FIGURE 18. Electromagnetic torque and resistant torque in two capacitors failure mode.

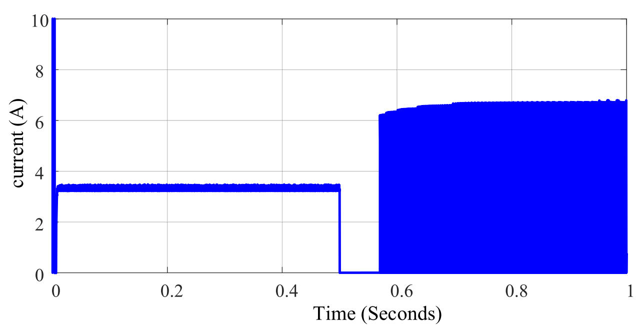

FIGURE 19. DC motor current in two capacitors failure mode.

As mentioned in references [23], [24], [25], current harmonics increase the temperature of the electric machine by 5%. Therefore, in this study, FTC is applied to solve these issues.

E. FAULTS DIAGNOSIS BASED MACHINE LEARNING

Machine learning and deep learning approaches are used in references [26], [27], [28].

In this study, fault diagnosis of multicellular converters using a machine learning-based semi-supervised fuzzy pattern matching approach during the failure of flying capacitors.

Three steps are considered in this section:

F. DATA PROCESSING

It tackles a big challenge, which is the extraction of useful data from massive amounts of raw simulation data.

In this work, different data can change with the failure of the flying capacitors, such as

- Vc1 and Vc2 (figure 11).
- Angular speed of electric motor (figure 12)
- Electromagnetic torque (figure 13)
- Stator current of electric motor (figure 14)

However, to differentiate between different scenarios of failure, V_{c1} and V_{c2} can be considered useful data.

G. DATA MANIPULATION

To make the selected useful data (Vc1 and Vc2) easier to exploit, the signal-to-noise ratio is improved using a low-pass filter (figures 20 and 21).

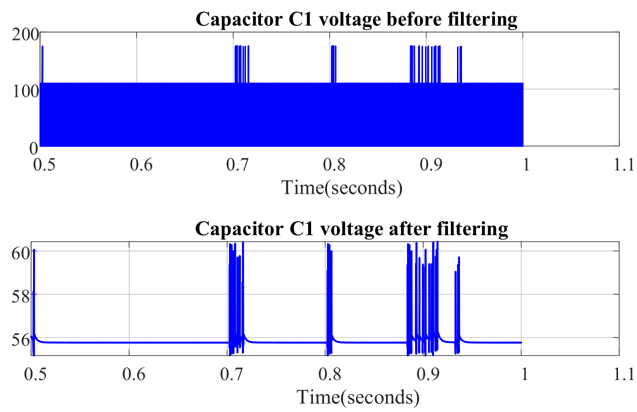

FIGURE 20. Voltages of capacitor C1 during failure.

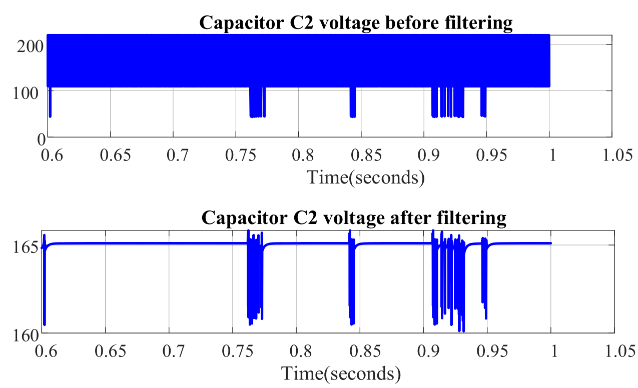

FIGURE 21. Voltages of capacitor C2 during failure.

After improving the signal-to-noise ratio of the useful data Vc1 and Vc2, figure 22 shows the feature space with two axes

(Vc1 and Vc2), which characterize the different operating modes (healthy, C1, C2, and C1 C2 failure modes).

According to figure 22, the selected feature space is highly discriminative for different operating modes to ensure good diagnostics.

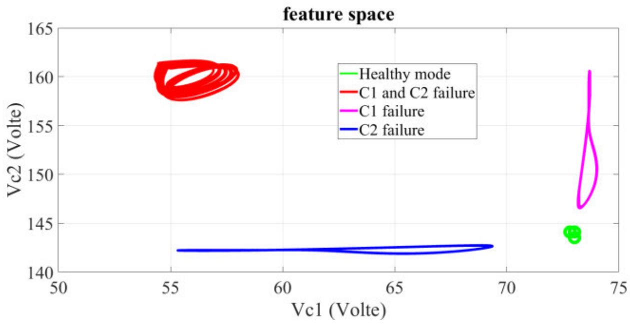

FIGURE 22. Voltages of capacitor C1 during failure.

H. FAULT CLASSIFICATION

This step aimed to create a classifier capable of assigning a new pattern representing the current operating conditions in one of the classes in the feature. These classes depict the healthy operating conditions and the faulty modes (C1, C2, C1 and C2), and occupy limited regions in the feature space (Figure. 22). To generate this classifier, a training set comprising historical data points for the normal and faulty operating conditions is used. Each data point is visualized as a pattern in the feature space and is specified by the voltages V_{C1} and V_{C2}. In this study, a dynamic classification method based on semi-supervised fuzzy pattern matching (SSFPM) is used [26].

SSFPM is a classification method that can learn decision boundaries between classes in unsupervised, supervised, and partially supervised learning settings [26]. The membership of data point measurements in supervised learning mode, representing the operating conditions of healthy conditions or failure states, is known in advance. In unsupervised learning mode, the membership of data points is missing. In the partially supervised learning mode, the membership of data points in known classes and operating modes is known in advance and can be used to learn the membership of new incoming data points in new classes, such as the occurrence of new failure modes. The SSFPM learns the decision function as follows:

- 1) Estimation of the probability densities (Prob_i^j, i = 1,.., c, j = 1,.., d) for each class C_i according to each feature or attribute j.
- 2) The probability densities are converted into possibility densities (Poss_i^j, i = 1,.., c, j = 1,.., d) using the Dubois and Prade probabilities for the possibility transformation.

For a new incoming data point x, SSFPM performs the classification as follows:

- Determine the possibility membership value poss_i^j of x according to each class C_i and each attribute j by projecting it onto the corresponding possibility density, Poss_i^j,
- Fusion of different membership values, poss_i^1., poss_i^d, of x, according to each class C_i using the fusion operator min. This fusion provides the membership value poss_i of x according to class C_i:
- Assignment of x to the class with the largest possible membership value.

Further details can be found in reference [26].

The membership function

$$\pi_i^j, i \in \{1, 2, 3, \ldots, c\}, j\{1, 2, 3 \ldots .., d\} \tag{21}$$

is estimated for each class i according to feature j. These membership functions allow the assignment of a pattern to a class, as follows: The membership value $\pi_i^j(x)$ of pattern x to class i according to feature j is calculated by projecting x into π_i^j. Then, the membership values $\pi_i^1(x)$, $\pi_i^2(x)$, $\pi_i^3(x)$, ... $\pi_i^d(x)$ of x to the class i according to all features $j = 1, \ldots$, d, are fused using the aggregation operator "minimum' in order to obtain the membership π_i^j of x to the class i. Membership values $\pi_1(x)$, $\pi_2(x)$, $\pi_3(x)$, ..., $\pi_c(x)$ of x for all classes was then calculated. x will Finally, x is assigned to the class for which it has the highest membership value. More details regarding the functioning of this method can be found in [26] and the references therein. This method was used because it is simple and has a low and constant classification time according to the database size [26].

Figure 23 show the proposed fault diagnosis method.

III. FAULT TOLERANT CONTROL

A. ONE FLYING CAPACITOR FAILURE

If the flying capacitor C2 is broken, we can eliminate one cell of the multicellular converter and consider a two-cell multicellular converter instead of three cells, with S_2 and S_3 having the same switching function.

The equation 6 can be expressed in two cells as the following:

$$\begin{aligned}
\begin{bmatrix} \dot{V}_{C1} \\ \dot{i}_P \end{bmatrix} &= \begin{bmatrix} 0 & 0 \\ 0 & \dfrac{-R_P}{L_P} \end{bmatrix} \begin{bmatrix} V_{C1} \\ i_P \end{bmatrix} \\
&\quad + \begin{bmatrix} \dfrac{-i_P}{C} & \dfrac{i_P}{C} \\ \dfrac{V_{C1}}{L_P} & \dfrac{V_{dc} - V_{C1}}{L_P} \end{bmatrix} \begin{bmatrix} S_1 \\ S_2 \end{bmatrix} + \begin{bmatrix} 0 \\ -\dfrac{K_\varphi}{L_P}\Omega \end{bmatrix} \\
x &= \begin{bmatrix} V_{C1} \\ i_P \end{bmatrix}, \quad x_{ref} = \begin{bmatrix} \dfrac{V_{dc}}{2} \\ i_P \end{bmatrix}, f_{f1} = \begin{bmatrix} 0 & 0 \\ 0 & \dfrac{-R_P}{L_P} \end{bmatrix}, \\
g_f &= \begin{bmatrix} \dfrac{-i_P}{C} & \dfrac{i_P}{C} \\ \dfrac{V_{C1}}{L_P} & \dfrac{V_{dc} - V_{C1}}{L_P} \end{bmatrix} \text{ and } H = \begin{bmatrix} 0 \\ -\dfrac{K_\varphi}{L_P}\Omega \end{bmatrix}
\end{aligned} \tag{22}$$

The error vector e is given by

$$e = x_{ref} - x = \begin{pmatrix} \frac{V_{dc}}{2} - V_{C1} \\ i_{Pref} - i_P \end{pmatrix} \tag{23}$$

This error e is considered as sliding surface of sliding mode control.

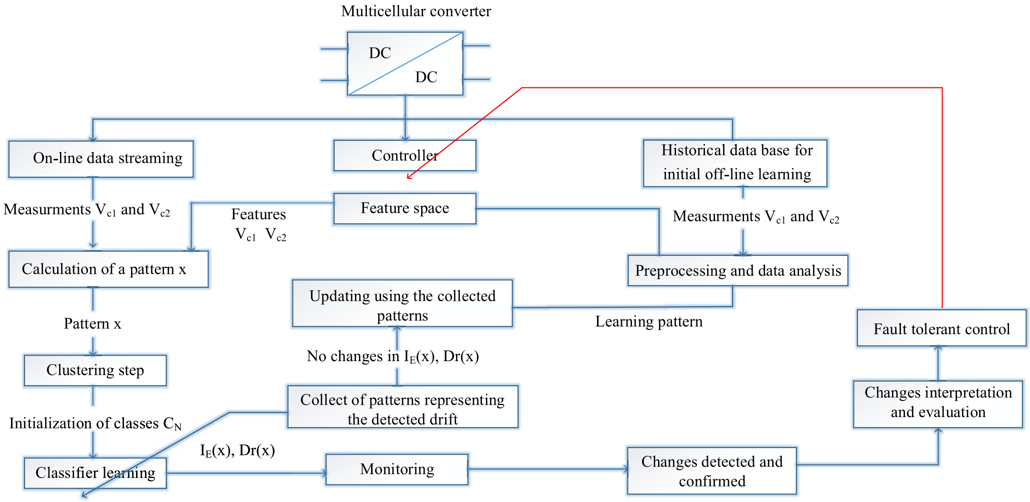

FIGURE 23. Fault diagnosis structure.

The same method is used to determine the switching functions with sliding mode control based on the Lyapunov stability.

$$S_1 = -sign\left[e^T\left(\frac{i_P}{C} + \frac{V_{C1}}{L_P}\right)\right]$$
$$S_2 = -sign\left[e^T\left(\frac{i_P}{C} + \frac{V_{dc} - V_{C1}}{L_P}\right)\right] \tag{24}$$

In this part, flying capacitor C_2 is considered to be defected. As shown in the simulation results, between 0.4S and 0.5S, the control without the FTC of the DC motor and after 0.5S, the FTC is introduced by eliminating the third cell with a defective flying capacitor, and the multicellular converter is considered as a two-cell converter with switching functions S_2 $=S_3$. Figure 24 shows the sliding mode control of the multicellular converter during the failure of a capacitor.

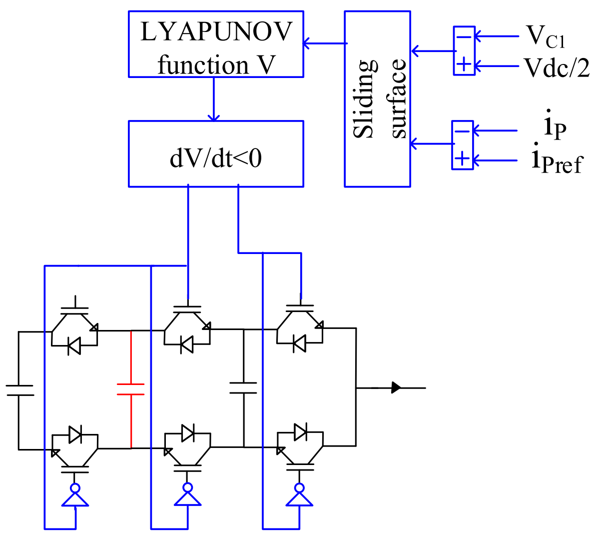

FIGURE 24. Multicellular converter with FTC in one capacitor failure mode.

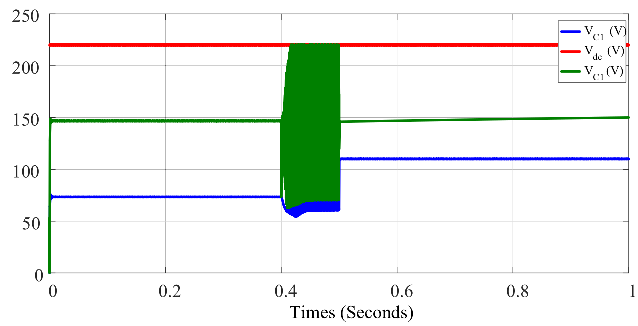

FIGURE 25. Flying capacitor voltages in one capacitors failure mode and FTC.

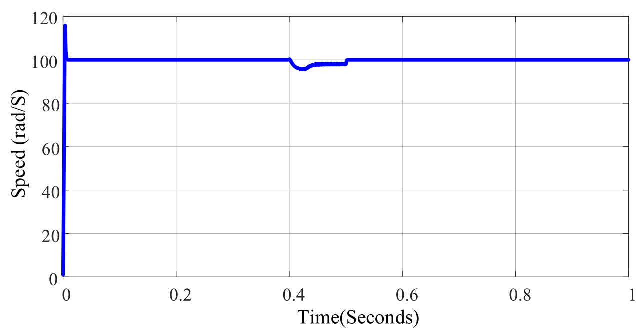

FIGURE 26. Angular speed of DC motor in in one capacitors failure mode and FTC.

When applying the FTC at instance 0.5S, the flying capacitor voltage is regulated at its new reference ($V_{C1} = V_{C1ref} = V_{dc}/2 = 110V$) as shown in Figure 25.

After applying the FTC, the multicellular converter generates the desired currents (Figure 28), and the DC motor operates at the desired speed and torque (Figure 26 and Figure 27).

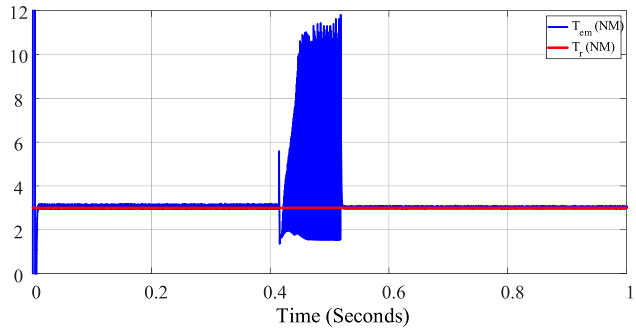

FIGURE 27. Electromagnetic torque and resistant torque in one capacitors failure mode and FTC.

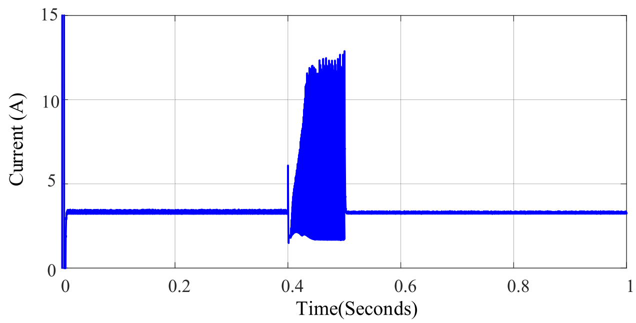

FIGURE 28. DC motor current in one capacitors failure mode and FTC.

B. TWO FLYING CAPACITORS FAILURE

If the two flying capacitors of the multicellular converter are defective, the FTC modifies the sliding mode control to hysteresis control, and the three cells have the same switching function ($S_1 = S_2 = S_3$).

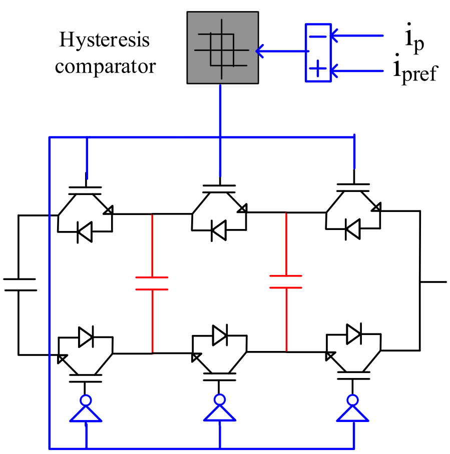

FIGURE 29. Multicellular converter with FTC and two capacitors failure mode.

In this part, the flying capacitors C_1 and C_2 are defected, and the multicellular converter is considered as a two-level converter with $S_1 = S_2 = S_3$ (Figure 29). At 0.5 S, the FTC is introduced with hysteresis control. The flying capacitor voltages are regulated at their reference ($V_{C1} = 110V$) as presented in Figure 30, and the angular speed, electromagnetic torque, and current of the DC motor are at their references during the application of the FTC (Figures 31-33)

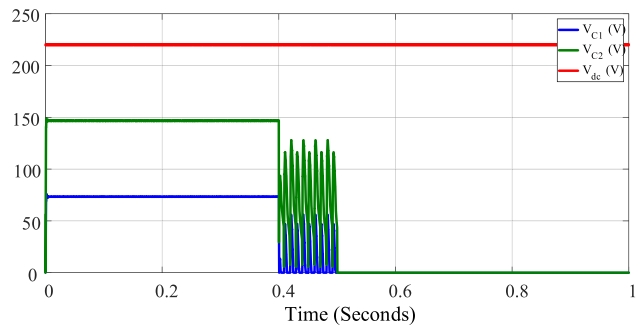

FIGURE 30. Flying capacitor voltages in one capacitors failure mode and FTC.

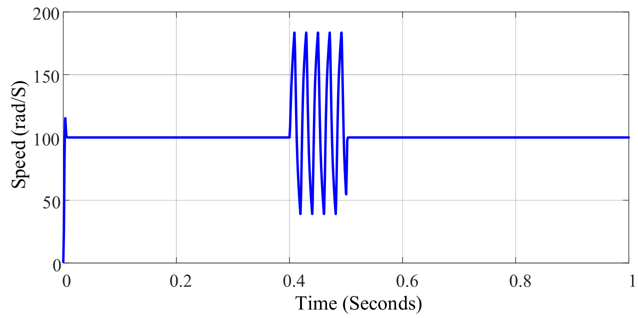

FIGURE 31. Angular speed of DC motor in two capacitors failure mode and FTC.

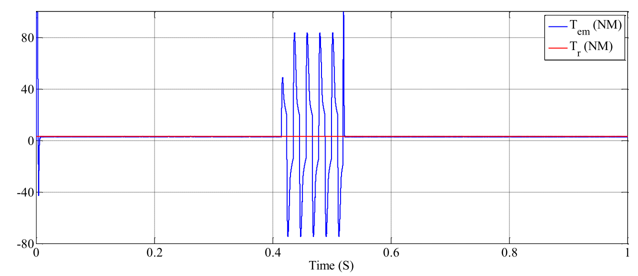

FIGURE 32. Electromagnetic torque and resistant torque in two capacitors failure mode and FTC.

In this work, during the faulty modes of multicellular converters, the simulation results prove that the fatigue problem mitigation, mechanical vibrations are reduced, harmonic currents in the stator windings are rejected, and consequently, the heat stress in the DC motor of the PV water-pumping system is minimized.

In [29] and [30], artificial intelligence-based machine learning algorithms such as support vector machines (SVM), artificial neural networks (ANN), and deep neural networks (DNN) were used to perform fault diagnosis of power electronic converters. In [26], SSFPM with reduced computational complexity and low learning and classification times was proposed.

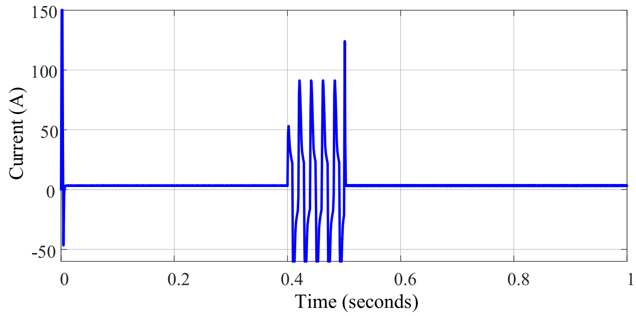

FIGURE 33. DC motor current in two capacitors failure mode and FTC.

A multicellular converter in a water-pumping system can present different operating modes over time. In pattern recognition methods, each mode is represented by a set of similar patterns that form a bounded region in the feature space (V_{C1} and V_{C2}), called a class. When a new incoming pattern is present, the membership function can recognize the class. The precision of this function depends on prior knowledge of the system functioning (reference voltage of V_{C1}, reference voltage of V_{C2}). In SSFPM, new states must be integrated and detected online in the dataset. When the information about some states is insufficient, missing information can be obtained from the new classified patterns, and the membership functions must be adapted online with the classification of new incoming patterns.

The SSFPM classification time (detection, integration, and adaptation online) was 3.5e-1S using a computer with an Intel (R) Core(TM) i5 and 2.50GHz.

IV. CONCLUSION

This paper presented a photovoltaic water pumping system using a multicellular power converter with fault-diagnosis-based machine learning and fault-tolerant control. Sliding mode and hysteresis controls are used in normal and faulty operations. The failure of one or two flying capacitors in a multicellular converter affects the operation of the water-pumping system as follows:

- Increase the current harmonics in the stator winding of the DC motor, which can increase the thermal stress.
- Increase the harmonics of electromagnetic torque, which can increase the mechanical vibrations.

The fault diagnosis and fault-tolerant control of multicellular converters presented in this work assure the supply in water when a failure occurs in the flying capacitors of multicellular converters with reduced mechanical vibrations and reduced thermal stress.

As a further direction, we propose a deep learning approach to enhance the performance of fault diagnosis and fault-tolerant control.

REFERENCES

[1] A. Allouhi, M. S. Buker, H. El-houari, A. Boharb, M. B. Amine, T. Kousksou, and A. Jamil, "PV water pumping systems for domestic uses in remote areas: Sizing process, simulation and economic evaluation," *Renew. Energy*, vol. 132, pp. 798–812, Mar. 2019, doi: 10.1016/j.renene.2018.08.019.

[2] B. Subudhi and R. Pradhan, "A comparative study on maximum power point tracking techniques for photovoltaic power systems," *IEEE Trans. Sustain. Energy*, vol. 4, no. 1, pp. 89–98, Jan. 2013, doi: 10.1109/TSTE.2012.2202294.

[3] S. Meunier, "Optimal design of photovoltaic water pumping systems for rural communities—A technical, economic and social approach," Dept. Elect., Opt., Bio-Phys. Eng., Thèse de doctorat de l'Université Paris-Saclay Préparée à l'Université Paris-Sud, Ecole Doctorale 575, 2019.

[4] D. H. Muhsen, T. Khatib, and T. E. Abdulabbas, "Sizing of a standalone photovoltaic water pumping system using hybrid multi-criteria decision making methods," *Sol. Energy*, vol. 159, pp. 1003–1015, Jan. 2018, doi: 10.1016/j.solener.2017.11.044.

[5] S. Murshid and B. Singh, "Single stage autonomous solar water pumping system using PMSM drive," *IEEE Trans. Ind. Appl.*, vol. 56, no. 4, pp. 3985–3994, Jul./Aug. 2020, doi: 10.1109/TIA.2020.2988429.

[6] A. Varshney, U. Sharma, and B. Singh, "Adaptive d-axis current control of RSyM for photovoltaic water pumping incorporating cross saturation," *IEEE Trans. Ind. Informat.*, vol. 16, no. 10, pp. 6487–6498, Oct. 2020, doi: 10.1109/TII.2020.2964905.

[7] B. Rouabah, H. Toubakh, and M. Sayed-Mouchaweh, "Fault tolerant control of multicellular converter used in shunt active power filter," *Electr. Power Syst. Res.*, vol. 188, Nov. 2020, Art. no. 106533, doi: 10.1016/j.epsr.2020.106533.

[8] B. Rouabah, L. Rahmani, H. Toubakh, and E. Duviella, "Adaptive and exact linearization control of multicellular power converter based on shunt active power filter," *J. Control, Autom. Electr. Syst.*, vol. 30, no. 6, pp. 1019–1029, Dec. 2019, doi: 10.1007/s40313-019-00510-w.

[9] A. K. Mishra and B. Singh, "An efficient control scheme of self-reliant solar-powered water pumping system using a three-level DC–DC converter," *IEEE J. Emerg. Sel. Topics Power Electron.*, vol. 8, no. 4, pp. 3669–3681, Dec. 2020, doi: 10.1109/JESTPE.2019.2943203.

[10] B. Rouabah, L. Rahmani, M. A. Mahboub, H. Toubakh, and M. Sayed-Mouchaweh, "More efficient wind energy conversion system using shunt active power filter," *Electr. Power Compon. Syst.*, vol. 49, nos. 4–5, pp. 321–332, Mar. 2021, doi: 10.1080/15325008.2021.1970285.

[11] B. Rouabah, "Contribution à l'amélioration des performances d'un filtre actif parallèle de puissance par l'utilisation d'un convertisseur multicellulaire," Ph.D. dissertation, Dept. Elect. Eng., Université Ferhat ABBAS—Sétif 1, 2021. [Online]. Available: http://dspace.univ-setif.dz:8888/jspui/handle/123456789/3803

[12] M. A. Mahboub, B. Rouabah, M. R. Kafi, and H. Toubakh, "Health management using fault detection and fault tolerant control of multicellular converter applied in more electric aircraft system," *Diagnostyka*, vol. 23, no. 2, pp. 1–7, Jun. 2022, doi: 10.29354/diag/151039.

[13] H. Toubakh and M. Sayed-Mouchaweh, "Hybrid dynamic classifier for drift-like fault diagnosis in a class of hybrid dynamic systems: Application to wind turbine converters," *Neurocomputing*, vol. 171, pp. 1496–1516, Jan. 2016, doi: 10.1016/j.neucom.2015.07.073.

[14] B. Rouabah, H. Toubakh, M. Djemai, L. Ben-Brahim, and M. R. Kafi, "New active fault tolerant control of multicellular converter," in *Proc. 7th Int. Conf. Environ. Friendly Energies Appl. (EFEA)*, Dec. 2022, pp. 1–6, doi: 10.1109/EFEA56675.2022.10063825.

[15] M. Benmiloud, A. Benalia, M. Djemai, and M. Defoort, "On the local stabilization of hybrid limit cycles in switched affine systems," *IEEE Trans. Autom. Control*, vol. 64, no. 2, pp. 841–846, Feb. 2019, doi: 10.1109/TAC.2018.2841806.

[16] S. Elmetennani, T. M. Laleg-Kirati, M. Djemai, and M. Tadjine, "New MPPT algorithm for PV applications based on hybrid dynamical approach," *J. Process Control*, vol. 48, pp. 14–24, Dec. 2016, doi: 10.1016/j.jprocont.2016.10.001.

[17] H. Toubakh, M. Sayed-Mouchaweh, M. Benmiloud, M. Defoort, and M. Djemai, "Self adaptive learning scheme for early diagnosis of simple and multiple switch faults in multicellular power converters," *ISA Trans.*, vol. 113, pp. 222–231, Jul. 2021, doi: 10.1016/j.isatra.2020.03.025.

[18] H. Toubakh, M. Sayed-Mouchaweh, A. Fleury, and J. Boonaert, "Hybrid dynamic data mining scheme for drift-like fault diagnosis in multicellular converters," in *Proc. 3rd Int. Conf. Technol. Adv. Electr., Electron. Comput. Eng. (TAEECE)*, Apr. 2015, pp. 56–61, doi: 10.1109/taeece.2015.7113600.

[19] A. Bouhafs, M. R. Kafi, L. Louazene, B. Rouabah, and H. Toubakh, "Fault-detection-based machine learning approach to multicellular converters used in photovoltaic systems," *Machines*, vol. 10, no. 11, p. 992, 2022, doi: 10.3390/machines10110992.

[20] C. M. Riley, B. K. Lin, T. G. Habetler, and G. B. Kliman, "Stator current harmonics and their causal vibrations: A preliminary investigation of sensorless vibration monitoring applications," *IEEE Trans. Ind. Appl.*, vol. 35, no. 1, pp. 94–99, Jan. 1999, doi: 10.1109/28.740850.

[21] A. Munoz R. and C. G. Nahmias, "Mechanical vibration of three-phase induction motors fed by nonsinusoidal currents," in *Proc. 3rd Int. Power Electron. Congress. Tech. (CIEP)*, Aug. 1994, pp. 166–172, doi: 10.1109/ciep.1994.494416.

[22] S.-P. Zhu, P. Yue, Z.-Y. Yu, and Q. Wang, "A combined high and low cycle fatigue model for life prediction of turbine blades," *Materials*, vol. 10, no. 7, p. 698, Jun. 2017, doi: 10.3390/ma10070698.

[23] J. Fouladgar and E. Chauveau, "The influence of the harmonics on the temperature of electrical machines," *IEEE Trans. Magn.*, vol. 41, no. 5, pp. 1644–1647, May 2005, doi: 10.1109/TMAG.2005.846113.

[24] B. Rouabah, H. Toubakh, M. R. Kafi, and M. Sayed-Mouchaweh, "Adaptive data-driven fault-tolerant control strategy for optimal power extraction in presence of broken rotor bars in wind turbine," *ISA Trans.*, vol. 130, pp. 92–103, Nov. 2022, doi: 10.1016/j.isatra.2022.04.008.

[25] B. Roubah, H. Toubakh, and M. Sayed-Mouchaweh, "Advanced fault-tolerant control strategy of wind turbine based on squirrel cage induction generator with rotor bar defects," in *Proc. Annu. Conf. Prognostics Health Manage. (PHM) Soc.*, Sep. 2019, pp. 1–8, doi: 10.36001/phm-conf.2019.v11i1.841.

[26] M. S. Mouchaweh, "Semi-supervised classification method for dynamic applications," *Fuzzy Sets Syst.*, vol. 161, no. 4, pp. 544–563, 2010.

[27] J. Zhang, Y. Zhao, F. Shone, Z. Li, A. F. Frangi, S. Q. Xie, and Z.-Q. Zhang, "Physics-informed deep learning for musculoskeletal modeling: Predicting muscle forces and joint kinematics from surface EMG," *IEEE Trans. Neural Syst. Rehabil. Eng.*, vol. 31, pp. 484–493, 2023, doi: 10.1109/TNSRE.2022.3226860.

[28] J. Zhang, Y. Li, W. Xiao, and Z. Zhang, "Non-iterative and fast deep learning: Multilayer extreme learning machines," *J. Franklin Inst.*, vol. 357, no. 13, pp. 8925–8955, Sep. 2020.

[29] Q. Wang, Y. Yu, H. O. A. Ahmed, M. Darwish, and A. K. Nandi, "Fault detection and classification in MMC-HVDC systems using learning methods," *Sensors*, vol. 20, no. 16, p. 4438, Aug. 2020, doi: 10.3390/s20164438.

[30] W. Gong, H. Chen, Z. Zhang, M. Zhang, and H. Gao, "A data-driven-based fault diagnosis approach for electrical power DC–DC inverter by using modified convolutional neural network with global average pooling and 2-D feature image," *IEEE Access*, vol. 8, pp. 73677–73697, 2020, doi: 10.1109/ACCESS.2020.2988323.

B. ROUABAH received the engineering degree from the University of Bordj Bou Arriridj, in 2009, and the Magister and Ph.D. degrees from the University of Setif 1, Algeria, in 2012 and 2021, respectively. Since 2020, he has been a Researcher with the University of Kasdi Merbah Ouargla, Algeria.

H. TOUBAKH received the engineering degree in electrical engineering from the University of Setif 1, Setif, Algeria, in 2010, and the master's degree in automation and computer engineering from National Polytechnic Institutes, Marseille, France, in 2012. His research interests include machine learning, wind turbine, and diagnosis and prognosis of industrial production systems using artificial intelligence techniques.

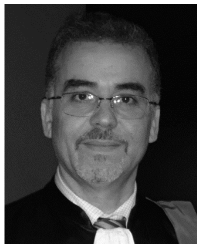

M. DJEMAI (Senior Member, IEEE) received the master's degree in electrical engineering from Ecole Nationale Polytechnique of Algiers, Algeria, in 1991, and the Ph.D. degree in control engineering from the University of Paris XI, CNRS-LSS, France, in 1996. He has been a Full Professor with the University of Valenciennes and Hainaut-Cambrésis, Valenciennes, France, since 2008. He was a Visiting Professor with Northumbria University, in 2010 and 2013. He is currently with the Laboratory of Industrial and Human Automation, Mechanics and Computer Science, CNRS, UMR 8201. His research interests include nonlinear control, observation, and fault detection theory, including hybrid system control, sliding-mode, and variable structure systems, with applications to power systems, robots, and vehicles. He is a member of IFAC TC 2.1 Control System and IFAC TC. 1.3 on Discrete Event and Hybrid Systems.

L. BEN-BRAHIM (Senior Member, IEEE) received the B.Sc. and M.Sc. degrees in electrical engineering from the National School of Engineers of Tunis, Tunisia, in 1985 and 1987, respectively, and the Ph.D. degree in electrical engineering from Yokohama National University, Yokohama, Japan, in 1991. From 1991 to 1997, he was with Toshiba Corporation, where he was engaged in the research and development of power electronics and motor drive systems. Since September 1997, he has been with the Industrial Technology Department, College of Technology, Qatar University. He was the Head of the Industrial Technology Department, from 1998 to 2005. In September 2005, he joined the Electrical Engineering Department, Qatar University. He was also the Industrial Electronics Chair of RasGas Company and the Head of the Electrical Engineering Department. He invented several new techniques for use in motor drives, power electronics, and sensors. These inventions are registered in more than 12 international patents. His current research interests include power electronics, renewable energy, electric vehicles, electric drives, and sensor and instrumentation. He is a member of IEE Japan. He is an Associate Editor of the *Journal of Electrical Engineering* (Springer) and an Editor of the *Electronics Journal* (MDPI).

RAYMOND GHANDOUR (Senior Member, IEEE) received the B.Eng. degree in computer and communication engineering from Holy Spirit University, Kaslik, Lebanon, in 2007, the M.S. degree in industrial control from Lebanese University, Beirut, Lebanon, in 2008, the M.S. degree in science of technology and information from the University of Technology of Compiegne, France, in 2008, and the Ph.D. degree in automatic control from the University of Technology of Compiegne, France, in 2011. In December 2011, he was a Postdoctoral Researcher with the University of Valenciennes and Hainaut-Cambresis (UVHC), Valenciennes, France. In December 2012, he was also a Postdoctoral Researcher with CETIM and the University of Technology of Compiegne. He joined the ALTRAN Group—ALTRAN Technologies—North Division, Lille, France, as the Director of Research and Development, in April 2013. He is currently an Assistant Professor with the American University of the Middle East, Kuwait. He has been conducting research in different areas, including control of hybrid vehicles, vehicle dynamics, signal processing, driving assistance systems, and modeling and control of nonlinear systems.